Science Bulletin 64 (2019) 136–141

Contents lists available at ScienceDirect

Science Bulletin

journal homepage: www.elsevier.com/locate/scib

Science Bulletin
www.scibull.com

Article

Composition engineering of Sb_2S_3 film enabling high performance solar cells

Yiwei Yin, Chunyan Wu, Rongfeng Tang, Chenhui Jiang, Guoshun Jiang, Weifeng Liu, Tao Chen *, Changfei Zhu *

CAS Key Laboratory of Materials for Energy Conversion, Department of Materials Science and Engineering, University of Science and Technology of China, Hefei 230026, China

ARTICLE INFO

Article history:
Received 17 October 2018
Received in revised form 19 November 2018
Accepted 4 December 2018
Available online 15 December 2018

Keywords:
Solar cell
Sb_2S_3
Thermal evaporation
Co-evaporation
Power conversion efficiency

ABSTRACT

Sb_2S_3 is a kind of stable light absorption materials with suitable band gap, promising for practical applications. Here we demonstrate that the engineering on the composition ratio enables significant improvement in the device performance. We found that the co-evaporation of sulfur or antimony with Sb_2S_3 is able to generate sulfur- or antimony-rich Sb_2S_3. This composition does not generate essential influence on the crystal structure, optical band and film formability, while the carrier concentration and transport dynamics are considerably changed. The device investigations show that sulfur-rich Sb_2S_3 film is favorable for efficient energy conversion, while antimony-rich Sb_2S_3 leads to greatly decreased device performance. With optimizations on the sulfur-rich Sb_2S_3 films, the final power conversion efficiency reaches 5.8%, which is the highest efficiency in thermal evaporation derived Sb_2S_3 solar cells.

1. Introduction

As a binary semiconducting compound, Sb_2S_3 has received increasing attention as light harvesting material for solar cell applications [1–3]. The simple chemical component possesses advantages in the phase and composition manipulation. In addition, Sb_2S_3 has high light absorption coefficient (1.8×10^5 cm^{-1} at 450 nm), excellent air and moisture stability and environmentally benign elements [4,5]. The band gap of Sb_2S_3 is around 1.7 eV, which is close to the ideal value predicted by Shockley-Queisser limit. In this regard, Sb_2S_3 can serve as either sole light absorption material or top cell light absorption material in tandem solar cells coupling with low band gap solar cells for obtaining even higher power conversion efficiency (PCE) [3].

The composition of light harvesting materials critically affects the final PCE of solar devices via multiple mechanisms. For example, in copper zinc tin sulfide (CZTS) solar cells, a copper-poor and zinc-rich phase is required [6,7]. The copper poor phase during the film fabrication can lead to well-crystallized and compact film, while the zinc-rich film could enhance the carrier transport. The copper indium gallium selenide (CIGS) also shows composition dependent photovoltaic performance [8–10]. A typical characteristic of CIGS material is its variable band gap, which can be changed by varying the Ga/(In + Ga) ratio. Furthermore, the transition from Cu-rich phase to slightly Cu-poor phase introduces defects that can limit the efficiency of solar cells. It is observed that for different light harvesting materials, there is different dependence of photovoltaic response on the composition. In general, it influences the crystallinity, film formability, defect state, carrier concentration and mobility, and so on. Ultimately, the composition engineering would determine the final PCE in a complete device.

In this research, we study the composition dependent photovoltaic properties of Sb_2S_3 solar cells. Recent years the fast development in the $Sb_2(S, Se)_3$ solar cells have been witnessed, including Sb_2S_3 and Sb_2Se_3 [11–13]. There have been intensive investigations on the device construction by utilizing various electron and hole transporting materials. Both solution and thermal evaporation have been applied for the synthesis of Sb_2S_3 light harvesting films. Following the successful deposition of Sb_2Se_3, rapid thermal evaporation method is adapted for the synthesis of high crystallinity Sb_2S_3 film with a PCE of 3.5% in the initial study [14]. Recently, Lan et al. [15] deposited Sb_2S_3 on Li-doped mesoporous TiO_2 using thermal evaporation and achieved a PCE of 4.42% which is the highest efficiency achieved by thermal evaporation derived Sb_2S_3 film. It is noted that the thermal deposition in literature all uses Sb_2S_3 as precursor materials, thus the manipulation on the composition of as-obtained Sb_2S_3 film is difficult. Furthermore, how the S/Sb atomic ratio affects the photovoltaic performance remains undiscovered. Herein, by controlling the ratios between Sb_2S_3 and S or Sb during thermal evaporation, we are able to identify this composition dependent photovoltaic performance.

* Corresponding authors.
E-mail addresses: tchenmse@ustc.edu.cn (T. Chen), cfzhu@ustc.edu.cn (C. Zhu).

https://doi.org/10.1016/j.scib.2018.12.013
2095-9273/

2. Experimental

2.1. Preparation of Sb_2S_3 thin film

Sb_2S_3 thin films were deposited on TiO_2 coated F:SnO_2 (FTO) glass by thermal evaporation under high vacuum (5×10^{-4} Pa). The 0.2 g S or Sb powder and 0.6 g Sb_2S_3 powder were loaded in two tungsten boats respectively. The deposition rate of each was raised to 1 and 3–4 nm/s before we opened the flapper. Thickness of the film was controlled about 100 nm by film thickness gauge. The deposition was carried out under room temperature. The as-deposited film was immediately transferred into N_2 glove box and annealed at hot plate at 300 °C for 2 min.

2.2. Device fabrication

Etched FTO glass was cleaned by IPA, acetone and de-ioned water and alcohol, treated by UV irradiation before use. The structure of our device can be described as glass/FTO/bl-TiO_2/TiO_2 array/Sb_2S_3/HTM/Au (HTM: hole transporting material). The compact TiO_2 layer was deposited onto cleaned FTO by spin-coating a mixture solution of 140 μL titanium isopropoxide, 2 mL ethanol, and 26 μL HCl (2 mol L^{-1}) method at 2,000 r min^{-1} for 40 s, followed by annealing at 550 °C for 60 min in air. TiO_2 arrays were then grew on compacted TiO_2 using hydrothermal method according to the reported method [16]. The obtained TiO_2 arrays were treated by 30 mmol L^{-1} $MgCl_2$ solution. After the deposition of Sb_2S_3, Spiro-OMeTAD was spin-coated at a speed of 3,000 r min^{-1} for 30 s, and baked at 100 °C for 10 min. Finally, Au counter electrode was deposited by a thermal evaporator under pressure of 5.0×10^{-4} Pa. The active area of the device was defined as 0.12 cm^2.

2.3. Characterizations and measurements

The crystallinity of samples were investigated by X-ray diffraction (XRD) using a Bruker Advance D8 diffractometer equipped with graphite-monochromatized Cu Kα radiation (λ = 1.5406 Å). The surface and cross-section morphologies of the Sb_2S_3 thin films were characterized by field emission scanning electron microscope (FE-SEM, Siron 200). UV–vis spectroscopy was characterized by an UV–vis-NIR 3600 spectrometer. The capacitance-voltage measurements were recorded from a Zahner Mess Systeme PP211 electrochemical workstation in the dark at 1,000 Hz from −0.5 to 1.0 V. Finally, current-voltage measurements were performed in a Newport Sol3A Class AAA Solar Simulator (450 W, Oriel, model 9119). Test was under an AM 1.5 illumination to produce a 100 mW cm^{-2} solar irradiation at room temperature. The external quantum efficiency (EQE, Model SPIEQ200) was measured using a single source illumination system (halogen lamp) combined with a monochromator. Electrochemical impedance spectroscopy measurements were performed using Zahner Mess Systeme PP211 electrochemical workstation at a bias potential of −0.65 V in dark with the frequency ranging from 1 Hz to 1 MHz. The X-ray photoelectron spectroscopy measurement was characterized by Escalab 250.

3. Results and discussion

We start our investigation from the composition controlled synthesis of Sb_2S_3 films. In accordance with the device fabrication, Sb_2S_3 film was synthesized onto the TiO_2 nanorods array. The detailed synthetic approach is depicted in Fig. 1. Prior to TiO_2 nanorods synthesis, a compact TiO_2 layer (c-TiO_2) with thickness of 50 nm was deposited on the FTO coated glass (Fig. 1a). The length of nanorods was controlled to be 100 nm on average (Fig. 1b). Here we emphasize that we also studied planar heterojunction Sb_2S_3 solar cells comparatively, i.e., in absence of TiO_2 nanorod, while this device structure can generate comparable PCE, the efficiency reproducibility is not as good as sensitized device structure. The nanorod based device would facilitate charge transport and deliver better performance. In this case, we adopt sensitized device configuration for detailed study.

The deposition of Sb_2S_3 was carried out under high vacuum (5×10^{-4} Pa) in a thermal evaporator (Fig. 1c). In brief, 0.2 g S or Sb powder and 0.6 g Sb_2S_3 powder were loaded in two tungsten boats respectively. By tuning heating current, the deposition rates of them were raised to 1 and 3–4 nm s^{-1}, respectively. The film thickness was controlled about 100 nm by film thickness gauge. During deposition, the target substrate was kept at room temperature. In this case, the deposited film is in amorphous form, as shown in Fig. S1 (online). To improve the crystallinity, as-deposited film was transferred into N_2 glove box and annealed at hot plate at 300 °C for 2 min. For the convenience of discussion, the pristine Sb_2S_3, sulfur doped Sb_2S_3 and antimony doped Sb_2S_3 are denoted as P-Sb_2S_3, S-Sb_2S_3 and Sb-Sb_2S_3, respectively.

The phase formation and crystallinity of as-deposited Sb_2S_3 films were firstly characterized by XRD. P-Sb_2S_3 exhibits diffractions at 15.6°, 17.5°, 24.8°, 28.5° and 32.4° (Fig. 2a), which are assigned as (0 2 0), (1 2 0), (1 3 0), (3 2 0), and (2 2 1) crystal planes of orthorhombic Sb_2S_3 phase (JCPDS No. 42-1393) [16,17]. With co-evaporation of S and Sb, the XRD characterizations display identical patters to that of P-Sb_2S_3, no impurity phases such as sulfur and antimony are identified. This observation indicates that sulfur and antimony are entered into the crystal lattice.

The composition was determined by X-ray photoelectron spectroscopy (XPS) as shown in Fig. 2c, d. The binding energy peaks at 161.1 and 162.3 eV are assigned to $2p_{3/2}$ and $2p_{1/2}$ of Sb_2S_3 [18,19]. It is worthy of noting that binding energy peaks at 164 and 528 eV belonging to element sulfur and antimony were not observed [20,21], confirming the elements are doped into the lattice of Sb_2S_3 film. As summarized in Table S1 (online), the atomic ratios of S/Sb in P-Sb_2S_3, Sb-Sb_2S_3, and S-Sb_2S_3 films are calculated to be 1.63, 1.42 and 1.72, respectively. This result suggests that by co-evaporation of sulfur and antimony, both S- and Sb-rich Sb_2S_3 films can be obtained. This tunability allows fundamental understanding as well as performance enhancement in Sb_2S_3 solar cells.

To study whether different S/Sb alters the band gap of the as-synthesized Sb_2S_3 films, we conducted UV–vis absorption spectroscopy characterization. Fig. 2b shows the UV–vis absorption spectra of P-Sb_2S_3, Sb-Sb_2S_3, and S-Sb_2S_3 films. The calculated band gap were all around 1.75, indicating that Sb_2S_3 film with S- or Sb-rich did not change the band gap of antimony sulfide films.

Furthermore, the morphology of P-Sb_2S_3, Sb-Sb_2S_3 and S-Sb_2S_3 were characterized by SEM. As shown in Fig. 3a–c, all of them display flat surface morphology with clear boundaries. There are no significant difference between the three kinds of Sb_2S_3, indicating that the co-evaporation of sulfur or antimony did not influence the crystallization and film growth, which is in contrast to the composition influenced crystal/morphology in CZTS solar cells [6]. In addition, since the Sb_2S_3 film was grown into the TiO_2 nanorods array, it serves as a scaffold to confine the growth of Sb_2S_3, contributing to the formation of similar morphology. By using TiO_2 nanorods arrays as substrate, on the other hand, the thickness of the Sb_2S_3 film can be well controlled. For all the samples, the cross-section SEM shows that the thickness of the films is around 100 nm (Fig. 3d–f). The similar film thickness allows us to make rational comparison in the device performance.

The complete device was fabricated by using Spiro-OMeTAD as HTM. Au film with thickness of 80 nm was finally deposited onto the HTM to form back contact. A cross section SEM of a typical device is shown in Fig. 4a. The current density (J)-voltage (V)

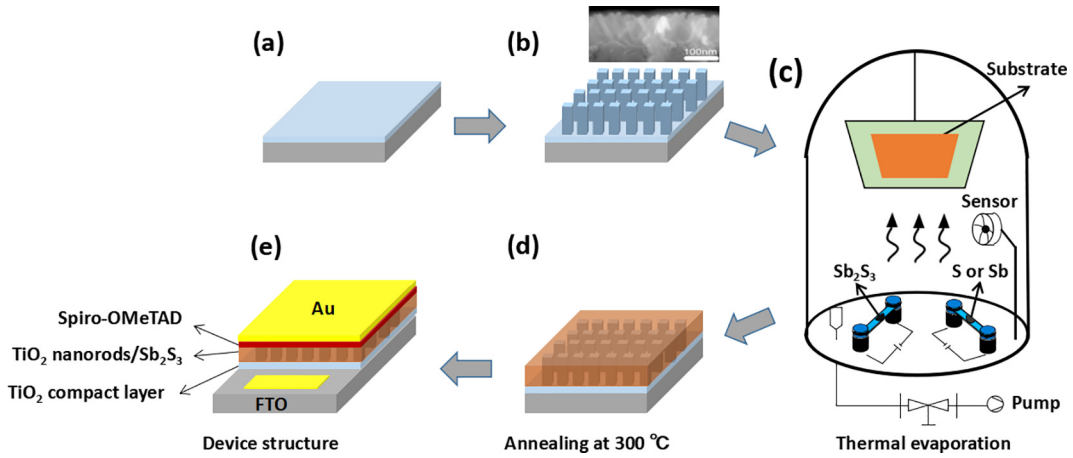

Fig. 1. (Color online) Schematic illustration of the fabrication process of Sb_2S_3 based device via thermal evaporation. (a) TiO_2 compact layer were spin coated on FTO coated glass. (b) TiO_2 nanorods were grown on TiO_2 compact layer via hydrothermal method. (c) Two sources of thermal evaporator are loaded with Sb_2S_3 and S or Sb for co-evaporation. (d) Annealing to improve the crystallinity of the film. (e) A complete device structure with Spiro-OMeTAD as HTM and Au film as metal contact.

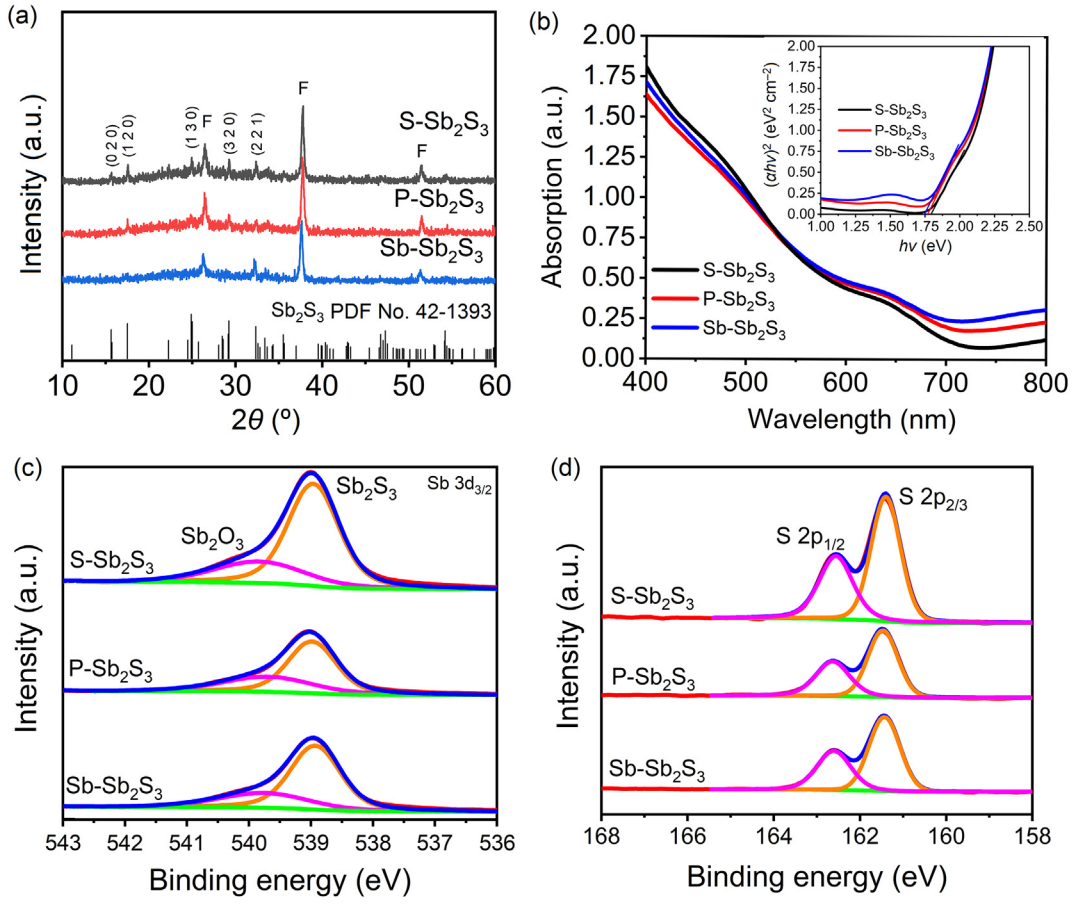

Fig. 2. (Color online) Structure and composition characterization of Sb_2S_3 films. XRD patterns (a) and UV–vis (b) absorption spectra of S-Sb_2S_3, P-Sb_2S_3 and Sb-Sb_2S_3. The inset in (b) shows the Tauc plot for band gap calculation of S-Sb_2S_3, P-Sb_2S_3 and Sb-Sb_2S_3 films. (c) and (d) High resolution core-level XPS spectra of Sb 3d$_{3/2}$ and S 2p in sample S-Sb_2S_3, P-Sb_2S_3 and Sb-Sb_2S_3, respectively.

behavior measured under one Sun illumination are displayed in Fig. 4b and the photovoltaic parameters are tabulated in Table 1. For the device based on P-Sb_2S_3 film, it delivers a short-circuit current density (J_{sc}) of 15.15 mA cm^{-2}, open-circuit voltage (V_{oc}) of 0.67 V and fill factor (FF) of 51.1%, corresponding to a PCE of 5.2%. This efficiency is higher than the reported device efficiency with thermal evaporation derived Sb_2S_3 film in literature which is generally below 5% [14,22,23]. With regard to sulfur doping, the device generates a PCE of 5.8%. Compared with the P-Sb_2S_3 based solar cell, both V_{oc} and J_{sc} are essentially improved. Remarkably, the V_{oc} reaches a value as high as 0.71 V, comparable to the highest value in solution processed Sb_2S_3 solar cell [2]. To affirm this result, we fabricated 12 devices of P-Sb_2S_3 and S-Sb_2S_3, respectively. Statistical performance data were shown in Fig. S2 (online).

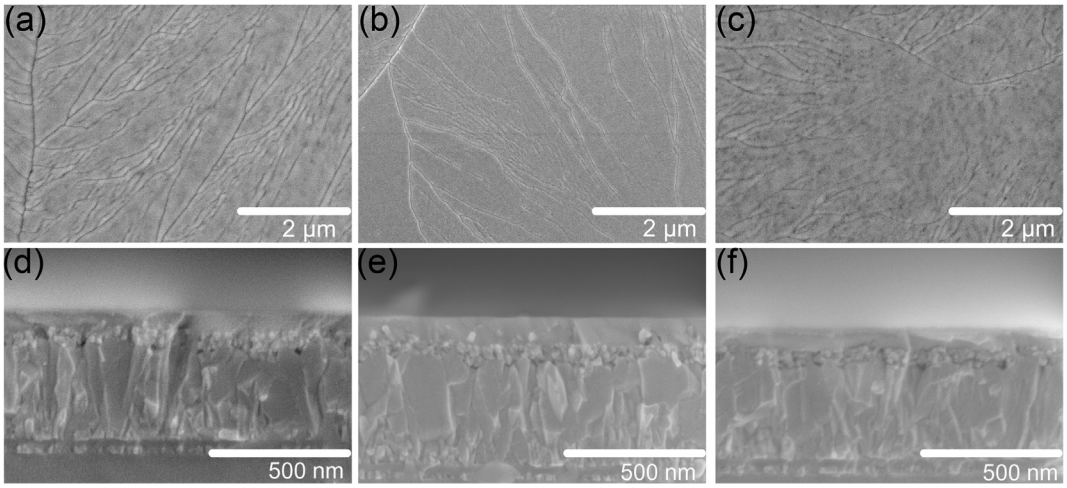

Fig. 3. SEM images of surface morphology of (a) S-Sb_2S_3, (b) P-Sb_2S_3 and (c) Sb-Sb_2S_3. Cross-sectional images of (d) S-Sb_2S_3, (e) P-Sb_2S_3 and (f) Sb-Sb_2S_3 on TiO_2 compact layer.

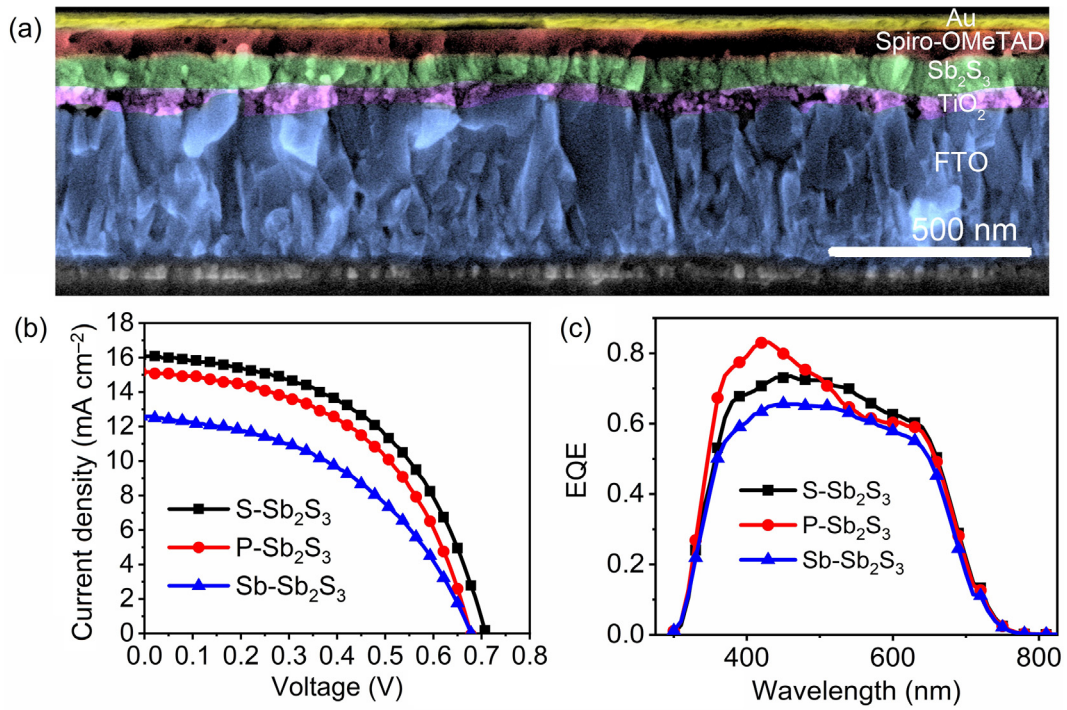

Fig. 4. (Color online) Device characterizations. (a) Cross-section SEM image of a complete device. (b) *J-V* curves and (c) EQE of the devices with S-Sb_2S_3, P-Sb_2S_3 and Sb-Sb_2S_3 as light absorption materials.

Table 1
Photovoltaic parameters of the devices based on S-Sb_2S_3, P-Sb_2S_3 and Sb-Sb_2S_3 as light absorbing materials, measured under one Sun AM 1.5G illumination.

Device	V_{oc} (V)	J_{sc} (mA cm^{-2})	FF (%)	PCE (%)
S-Sb_2S_3	0.71	16.11	50.72	5.8
P-Sb_2S_3	0.67	15.15	51.07	5.2
Sb-Sb_2S_3	0.69	12.83	48.36	4.3

Obviously, the average efficiency of P-Sb_2S_3 cells is 4.9% while the average efficiency of S-Sb_2S_3 cells is 5.3%. The S doping can raise the V_{oc} and FF of devices. However, the doping of antimony in Sb_2S_3 leads to the PCE reducing to 4.3%. In this case, the V_{oc} (0.69 V) is similar to that of P-Sb_2S_3 based device (0.67 V), while the J_{sc} and FF are considerably decreased. We further scan the cell with different direction as shown in Fig. S3 (online). No obvious hysteresis was observed in our device.

The EQE of the device are shown in Fig. 4c. All of the devices shows identical spectral region from 300 to 780 nm. The devices based on P-Sb_2S_3 and S-Sb_2S_3 show higher photocurrent generation than that of Sb-Sb_2S_3 device. This evolution is in consistence with the current density change in the *J-V* measurement.

Capacitance-voltage (*C-V*) profile was usually applied to detect the charge carrier concentration and built-in potential (V_{bi}) for the devices. The plots of $1/C^2$-*V* are shown in Fig. 5a. Approximately, we utilize parallel-plate capacitor model to describe the abrupt p-n heterojunction capacitance. The charge carrier concentration and V_{bi} were calculated according to the following equations:

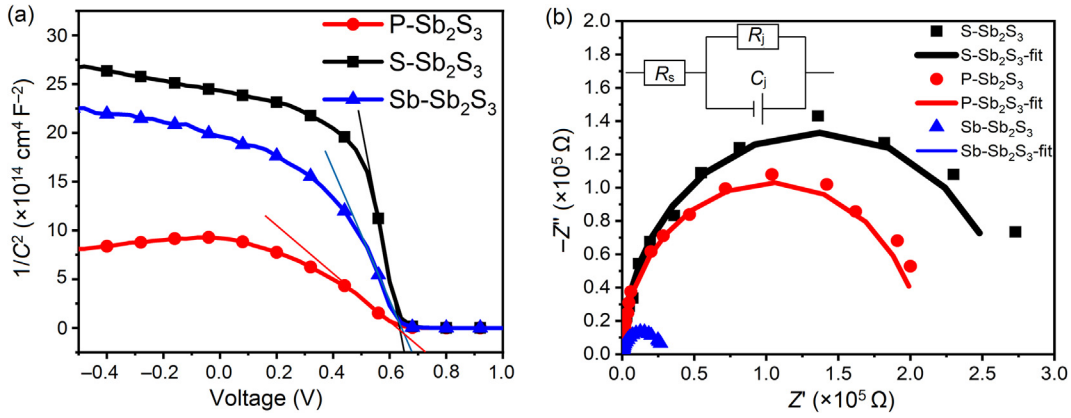

Fig. 5. (Color online) Electrochemical characterizations of the devices. (a) $1/C^2$-V curves and (b) Nyquist plots of the device based on S-Sb_2S_3, P-Sb_2S_3 and Sb-Sb_2S_3.

$$N_{A,p} = \frac{-2N_{D,n}\varepsilon_{r,n}}{\frac{d(1/C^2)}{dV} qN_{D,n}\varepsilon_{r,p}\varepsilon_{r,n}A^2\varepsilon_0 + 2\varepsilon_{r,p}}, \quad (1)$$

$$\frac{1}{C^2} = \frac{2(V_{bi} - V)}{qA^2\varepsilon_0\varepsilon_{r,p}N_{A,p}}, \quad (2)$$

where N_A, p, V, V_{bi}, q, ε_0, ε_r, and A represent carrier concentration, bias voltage, built-in potential, elementary charge, vacuum permittivity, relative permittivity, and device area, respectively [24]. According to the equation, the carrier concentration was proportional to the slope of $1/C^2$-V curves. The calculated carrier concentrations of P-Sb_2S_3, S-Sb_2S_3, and Sb-Sb_2S_3 based devices are 1.18×10^{16}, 1.16×10^{15} and 2.66×10^{15} cm^{-3}, all of which are suitable for a high performance solar device. Interestingly, we observe that either Sb or S co-evaporation would decrease the carrier concentration. Since Sb and Bi are at the same group and Sb_2S_3 and Bi_2S_3 possess identical crystal structure, we analyze the carrier concentration by referring to the defect properties of Bi_2S_3 as shown in first-principle study [25]. Herein, we propose that the increasing content of Sb will reduce the formation energy of S vacancies and Sb_s antisites. Their low formation energy at neutral state and hard ionization leads to the low concentration of free electron carriers. For S rich environment, it is easy to generate interstitial S as defect which acts as S vacancies and Sb_s antisites. This may explain the low carrier concentration after co-evaporation. However it is acknowledged that the detailed behavior of Bi_2S_3 may not transfer to Sb_2S_3 and therefore a dedicated density functional theory (DFT) study of Sb_2S_3 would be valuable.

To further investigate this phenomenon, we applied electrochemical impedance spectroscopy (EIS) to characterize the carrier transport behaviors. Impedance spectroscopy of devices was recorded at a potential of −0.65 V and frequency ranging from 1 Hz to 1 MHz. The results were shown in Fig. 5b, where the inset shows corresponding equivalent circuit model. R_s, R_{rec} and C_j represent the series resistor, recombination resistor, and chemical capacitance, respectively. R_s is correlated with internal resistance of the devices, which are 18.7, 17.6 and 26.5 Ω for devices based on P-Sb_2S_3, S-Sb_2S_3, and Sb-Sb_2S_3, respectively. The device with S-Sb_2S_3 shows reduced R_s when compared with the other two. The essentially increased R_s in Sb-Sb_2S_3 based device is one of the reasons for poor device performance, while the device with S-Sb_2S_3 displays smallest R_s. The value of recombination resistance R_{rec} is associated with the diameter of arc. Devices based on P-Sb_2S_3, S-Sb_2S_3, and Sb-Sb_2S_3 light harvesting materials exhibit R_{rec} of 210, 260 and 30 kΩ, respectively. Notably, the S-Sb_2S_3 device shows a higher R_{rec} than the other two. Meanwhile, the Sb-Sb_2S_3 device exhibits lowest R_{rec}. Accordingly, both the smallest R_s and highest R_{rec} contribute to the best performance of S-Sb_2S_3 device.

4. Conclusions

In conclusion, we demonstrate that the co-evaporation of element sulfur or antimony with Sb_2S_3 is able to manipulate the composition of Sb_2S_3 films. The structural analysis shows that sulfur or antimony can incorporated into the crystal lattice upon post-annealing. With this method, sulfur- or antimony-rich Sb_2S_3 films are obtained. Our research discovers that this elemental manipulation does not notably affect the band gap, morphology and crystallinity of the final films, while the carrier concentration and charge transport properties are essentially altered. Ultimately, sulfur-rich Sb_2S_3 film based device shows high carrier concentration, reduced recombination probability when compared with pristine and antimony-rich Sb_2S_3 based devices. A device efficiency of 5.8% is thus obtained, which is higher than direct deposition from Sb_2S_3 in our study and reported results.

Conflict of interest

The authors declare that they have no conflict of interest.

Acknowledgments

This work was supported by the Fundamental Research Funds for the Central Universities (WK2060140023, CX3430000001, and WK2060140024), the Major/Innovative Program of Development Foundation of Hefei Center for Physical Science and Technology (2016FXZY003), and the National Natural Science Foundation of China (U1732150).

Appendix A. Supplementary data

Supplementary data to this article can be found online at https://doi.org/10.1016/j.scib.2018.12.013.

References

[1] Chang JA, Im SH, Lee YH, et al. Panchromatic photon-harvesting by hole-conducting materials in inorganic-organic heterojunction sensitized-solar cell through the formation of nanostructured electron channels. Nano Lett 2012;12:1863–7.
[2] Choi YC, Lee DU, Noh JH, et al. Highly improved Sb_2S_3 sensitized-inorganic-organic heterojunction solar cells and quantification of traps by deep-level transient spectroscopy. Adv Funct Mater 2014;24:3587–92.
[3] Kondrotas R, Chen C, Tang J. Progress and prospects of Sb_2S_3-based thin film and tandem solar cells. Joule 2018;2:857–78.

[4] Itzhaik Y, Niitsoo O, Page M, et al. Sb_2S_3-sensitized nanoporous TiO_2 solar cells. J Phys Chem C 2009;113:4254–6.
[5] Wang X, Tang R, Wu C, et al. Development of antimony sulfide-selenide $Sb_2(S,Se)_3$-based solar cells. J Energy Chem 2017;27:713–21.
[6] Tanaka K, Fukui Y, Moritake N, et al. Chemical composition dependence of morphological and optical properties of Cu_2ZnSnS_4 thin films deposited by sol-gel sulfurization and Cu_2ZnSnS_4 thin film solar cell efficiency. Solar Energy Mater Solar Cells 2011;95:838–42.
[7] Chen S, Gong X, Walsh A, et al. Defect physics of the kesterite thin-film solar cell absorber Cu_2ZnSnS_4. Appl Phys Lett 2010;96:021902.
[8] Dhere NG. Present status and future prospects of CIGSS thin film solar cells. Solar Energy Mater Solar Cells 2006;90:2181–90.
[9] Lundberg O, Edoff M, Stolt L. The effect of Ga-grading in CIGS thin film solar cells. Thin Solid Films 2005;480:520–5.
[10] Jung S, Ahn S, Yun JH, et al. Effects of Ga contents on properties of CIGS thin films and solar cells fabricated by co-evaporation technique. Curr Appl Phys 2010;10:990–6.
[11] Wang L, Li DB, Li K, et al. Stable 6%-efficient Sb_2Se_3 solar cells with a ZnO buffer layer. Nat Energy 2017;2:17046.
[12] Choi YC, Lee YH, Im SH, et al. Efficient inorganic-organic heterojunction solar cells employing $Sb_2(S_x/Se_{1-x})_3$ graded-composition sensitizers. Adv Energy Mater 2014;4:1301680.
[13] Christians JA, Leighton DT, Kamat PV. Rate limiting interfacial hole transfer in Sb_2S_3 solid-state solar cells. Energy Environ Sci 2014;7:1148–58.
[14] Deng H, Yuan S, Yang X, et al. Efficient and stable TiO_2/Sb_2S_3 planar solar cells from absorber crystallization and Se-atmosphere annealing. Mater Today Energy 2017;3:15–23.
[15] Lan C, Luo J, Lan H, et al. Enhanced charge extraction of Li-doped TiO_2 for efficient thermal-evaporated Sb_2S_3 thin film solar cells. Materials 2018;11:355.
[16] Tang R, Wang X, Jiang C, et al. Vacuum assisted solution processing for highly efficient Sb_2S_3 solar cells. J Mater Chem A 2018;6:16322–7.
[17] Tang R, Wang X, Jiang C, et al. N-type doping of Sb_2S_3 light harvesting film enabling high efficiency planar heterojunction solar cells. ACS Appl Mater Interfaces 2018;10:30314–21.
[18] Itzhaik Y, Bendikov T, Hines D, et al. Band diagram and effects of the kscn treatment in TiO_2/Sb_2S_3/CuSCN eta cells. J Phys Chem C 2015;120:31–41.
[19] Fu Q, Yang L, Wang W, et al. Synthesis and enhanced electrochemical catalytic performance of monolayer $Ws_{2(1-x)}Se_{2x}$ with a tunable band gap. Adv Mater 2015;27:4732–8.
[20] Choi YC, Seok SI. Efficient Sb_2S_3-sensitized solar cells via single-step deposition of Sb_2S_3 using S/Sb-ratio-controlled $SbCl_3$-thiourea complex solution. Adv Funct Mater 2015;25:2892–8.
[21] Zakaznova-Herzog VP, Harmer S, Nesbitt H, et al. High resolution xps study of the large-band-gap semiconductor stibnite (Sb_2S_3): structural contributions and surface reconstruction. Surface Sci 2006;600:348–56.
[22] Lan C, Liang G, Lan H, et al. Microstructural and optical properties of Sb_2S_3 film thermally evaporated from antimony pentasulfide and efficient planar solar cells. Phys Status Solidi RRL 2018;12:1800025.
[23] Escorcia-García J, Becerra D, Nair M, et al. Heterojunction Cds/Sb_2S_3 solar cells using antimony sulfide thin films prepared by thermal evaporation. Thin Solid Films 2014;569:28–34.
[24] Yuan S, Deng H, Yang X, et al. Postsurface selenization for high performance Sb_2S_3 planar thin film solar cells. ACS Photon 2017;4:2862–70.
[25] Han D, Du MH, Dai CM, et al. Influence of defects and dopants on the photovoltaic performance of Bi_2S_3: first-principles insights. J Mater Chem A 2017;5:6200–10.

Yiwei Yin received his B.S. degree in Huazhong University of Science and Technology in Material Science and Engineering (2016), and now he is pursuing his Doctoral degree in University of Science and Technology of China, working on new solar energy materials and solar cells.

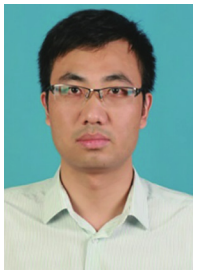

Tao Chen received his Ph.D. degree in Chemistry from Nanyang Technological University (Singapore) in 2010. From 2011 to 2015, he was working in the Chinese University of Hong Kong as a research assistant professor. He is now a professor at the Department of Materials Science and Engineering, University of Science and Technology of China. His research interests include materials science, the fabrication and engineering of antimony sulfide-selenide ($Sb_2(S,Se)_3$) solar cells.

Changfei Zhu received his B.S. and Ph.D. degrees both from University of Science and Technology of China (USTC) in 1984 and 1990, respectively. He has been working in the Department of Materials Science and Engineering of USTC since 1990 and was promoted to full professor in 2000. His research interests include the fundamental study and application of transitional metal oxide, wide band gap semi-conductor and thin film solar cells.